INFLUENCE OF DIE TEMPERATURE CONTROL ON SOLIDIFICATION AND THE CASTING PROCESS

T. Vossel [iD], N. Wolff, B. Pustal, and A. Bührig-Polaczek
Foundry Institute, RWTH Aachen University, Intzestraße 5, 52072 Aachen, Germany

Abstract

Permanent mold metal casting processes use tempering with oil, water or air as state-of-the-art method for temperature control of certain regions. This approach aims at either creating certain temperature gradients inside the die thus leading to better casting quality or cools down critical hotspots in order to decrease cycle times or increase service life. In order to perform an investigation on the influences of oil tempering on a permanent die and the solidification of the aluminum alloy A356, an experimental setup is used with measurement instrumentation for recording temperatures inside the melt and die as well as recording the movement of the die and the casting, thus enabling a gap width determination and measuring the contact pressure present on an inner core. A thermomechanical simulation of the solidification also is performed representing the processes occurring inside the experimental setup and extending the available data beyond the information locally provided at the experimental measuring positions. This approach allows for an evaluation of the influence of oil tempering on the solidification process, the thermal conditions inside of the casting, die, and core, and describes the behavior of a one-sided cooling of a comparatively large melt volume as well as the influences on a region with two-sided heat extraction affecting a smaller melt volume.

Keywords: *oil tempering, temperature control, A356, thermal analysis, gap size, contact pressure*

Introduction and Background

The casting process represents a complex interaction of numerous physical effects. Two main factors for influencing the casting process exist: On the one hand, there is the possibility of influencing the present metallurgy which is about changing the material and casting properties of the casted alloy. Depending on which alloy (system) is used, the means and possibilities for change differ, but for an Al–Si alloy, grain refinement and modification would be the two usual means of exerting influence on the metallurgical side. Apart from the positive influence of those two treatments on mechanical properties, the grain refinement of the primary α mixed crystal and modification of the eutectic silicon leads to improved casting properties.[1–4] On the other hand, besides the choice of the casting process itself (gravity casting, high-pressure die casting, etc.), the chosen process parameters are essential for obtaining a sound casting. In general, thermal factors have an impact on casting quality and mold service life.[5] For a given permanent mold casting system, temperature control of the die is state-of-the-art. Here, either the heating of certain areas or a cooling can be used to both control the heat balance and reach desired temperatures faster. This paper presents the effects of variation of die temperature control temperatures applied in a gravity die casting process using the A356 (AlSi7Mg0.3) cast alloy. As the changes of the microstructure due to differences in cooling rates have been sufficiently documented as well as the impact of the cooling rate on grain refinement and modification,[6] the discussion's focus will be on the process-related influences. A thermal analysis will be performed in order to identify the characteristics of the solidification.[7,8] This way the exact changes and characteristic effects that can be transferred to other castings and processes shall be depicted. For this, an experimental measurement as well as a thermomechanical simulation using the software Abaqus will be performed delivering results beyond the local measurement positions or limitations of the measurement setup.

Experimental Setup

The experimental setup used to examine the influence of die temperature control on the casting process is shown schematically in Figure 1.[9] Here, a "bowl," i.e., a cylindrical and thus rotationally symmetric part, is casted on an inner core. The aluminum alloy A356 used in the experiments came in the form of premade ingots already featuring a (Ti-) grain refinement and (Sr–) modification (cf. Table 1). After degassing with Ar-gas, the alloy is gravity casted into the central feeder inside the sand cover at 720 °C. The filling time of the casting process amounted to approx. 5 s. While the outer die as well as the inner core is made of steel, the actual outer wall of the casting cavity itself consists of copper inserts which are put into the outer steel die and are temperature controlled via cooling channels filled with oil. The feeder also acting as sprue is built in the form of a sand cover that is put on top of the permanent mold. This way the heat extraction is a quasi-one-dimensional process due to the rotational symmetry, and heat is transferred either to the inner steel core or the outer copper inserts. Three quantities are measured by the applied instrumentation (cf. Figure 2 on the left): Type-K thermocouples ("TCs") measure the temperature development inside of the die walls as well as inside the melt. The exact positions are shown in Figure 2 on the right. Via quartz rods inserted into both the die and the melt, the second quantity of local material movement is measured. Linear variable differential transformers (="LVDTs") outside of the mold record the respective movement which is transmitted to them via the rods. This also enables the determination of the air gap that forms between the copper inserts and the casting as a gap forms along the entire outer cavity wall due to the volume shrinkage of the casting. Analogously, the contact pressure on the surface of the inner core is being measured via an inserted quartz transferring the respective forces to a load cell thus representing the third measured quantity.

Concerning the experimental procedure, in addition to mounting the respective thermocouples and glass rods, the mold walls were finished with a ceramic, glimmer-based foundry coating via spraying. The cooling channels of the
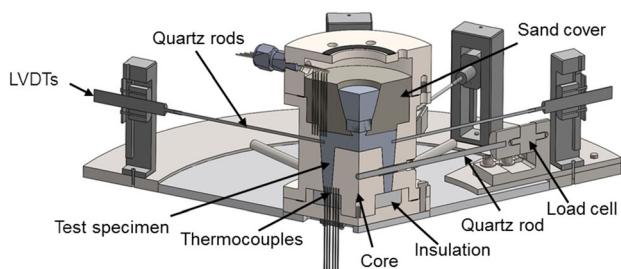
Figure 1. Experimental setup for casting the "bowl" geometry with measurement instrumentation for temperature, gap size and contact pressure.[9]

Table 1. Chemical Composition of the A356 Ingots [mass%]

Si	Fe	Cu	Mn	Mg	Zn	Ti	Other
6.5–7.5	0.12	0.02	0.05	0.3–0.45	0.07	0.18	Sr

copper inserts were filled with oil, and each insert's channels were tempered by a separate hot cooling aggregate. The oil tempering serves both as heating to increase the die temperature to the desired level and cooling once the molten metal has been cast and the ongoing oil tempering works as cooling for the die. Figure 3 on the left shows the channel layout together with the result of a numerical simulation of the resulting temperature field inside the insert during heating via hot oil of constant temperature. The used channel design was realized via drill holes and shows a nearly homogenous temperature distribution with minor hotspots along the presence of the actual channels. Actual oil tempering temperatures 30, 100, 200 and 300 °C were chosen, thus covering a range from room temperature up to high die temperature, whereas the upper limit of 300 °C was predetermined by the oil's evaporating temperature of around 370 °C which has to be avoided to prevent damage caused by sudden gas expansion. The chosen temperature for the oil remains constant during the respective experiment for both the heating phase prior to casting the aluminum alloy and the cooling phase after the melt has been casted. Regarding the thermocouples, all 12 measuring positions depicted in Figure 2 were always fitted with Type-K thermocouples in all experiments. For the LVDT measurements of the casting and die, the movements always were measured at three positions circularly around the experimental setup at identical height. Pressure measurement only occurred at one position. Due to the elaborate preparations needed and the loss of the quartz rods for every casting experiment performed, only one component was cast for each oil tempering setting.

The geometries of the experimental setup were transferred into the software Abaqus in order to perform solidification simulations. By using the given symmetries, it was possible to restrict the needed geometry to one-third of the total setup (cf. Figure 3 on the right). The chosen simulation model applied enabled thermomechanical calculations, thus allowing for local information of stresses and strains during the solidification and cooling process which enables the determination of gap sizes and contact pressures within the simulation—especially for the heat transfer coefficient calculations. In order to model the liquid–solid phase change, an algorithm for the release of latent heat is implemented into the Abaqus HETVAL routine. Implemented as temperature-dependent development of the fraction solid, a 3D thermodynamically coupled phase field simulation of the microstructure development under thermal boundary conditions as present in the actual
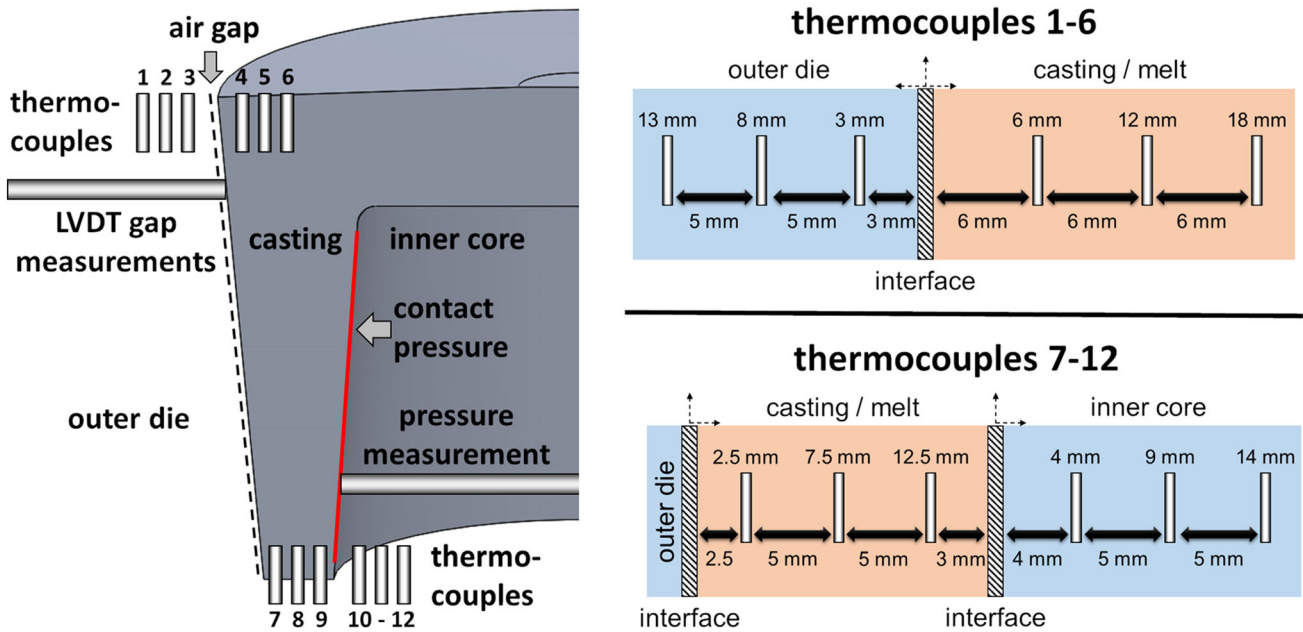
Figure 2. Overview of the measurement instrumentation (left) and exact positions of the thermocouples (right).
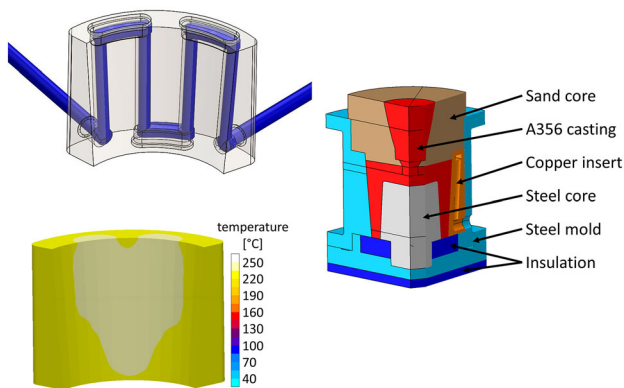

Figure 3. Cooling channel design inside the copper inserts and simulation of the developing temperature field during heating process (left) and overview of the Abaqus simulation setup (right).

Figure 4. Solid fraction as function of temperature obtained via coupled phase field simulations with Micress.[11]

experiment is performed to describe the ongoing solidification.[10] Here, the phenomena during the solidification of a eutectic A356 alloy are modeled starting with heterogeneous nucleation followed by a primary and finally eutectic solidification accommodating these effects in the temperature-dependent data set for the fraction solid development.[11] Figure 4 shows the resulting development of fraction solid over temperature.

Results

In order to describe the influence of the different die temperature control temperatures (i.e., the tempering of the die) on the casting pro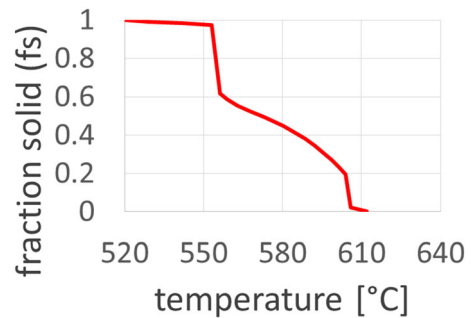cess, the temperature measurements inside the melt as recorded during the experiments will be discussed. Figures 5 and 6 show the cooling curves for the upper and lower measurement for the respective close to die position (thermocouple 4 and 7 in Figure 2). The data presented have been selected so that they are only used from the point in time when the respective thermocouple has reached its maximum measured temperature as a result of melt contact. This procedure takes into account the inertia of the thermocouples, which do not yet provide reliable data during the first measurements of a temperature rise. Only after they have reached the temperature level of the surrounding melt and this way have settled sufficiently, do they no longer deliver strongly fluctuating values and the data determined subsequently can be used for evaluation. The two measurement positions considered differ in terms of their cooling conditions, which are reflected in the graphs shown. Basically, the rotationally symmetrical geometry of the experimental setup causes a quasi-one-
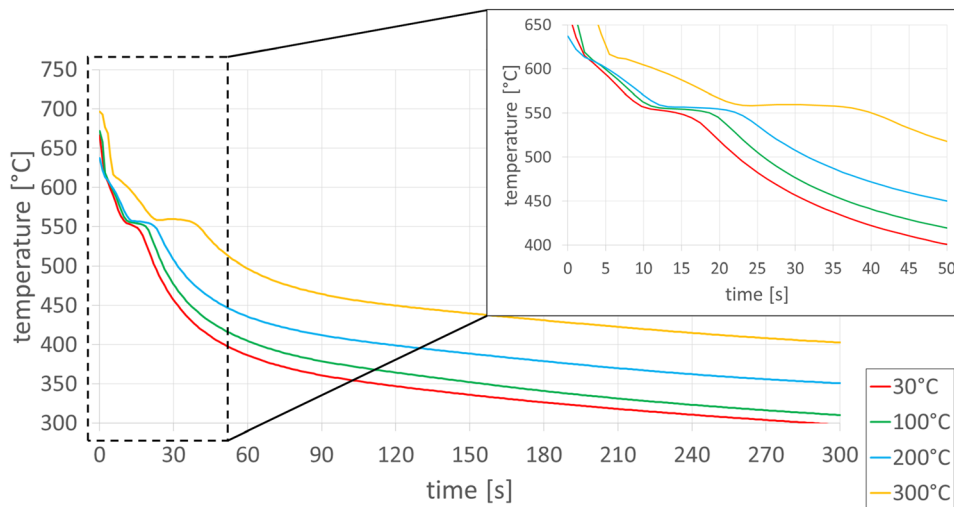
Figure 5. Cooling curves for lower, close to die (TC7) measuring position inside the melt.
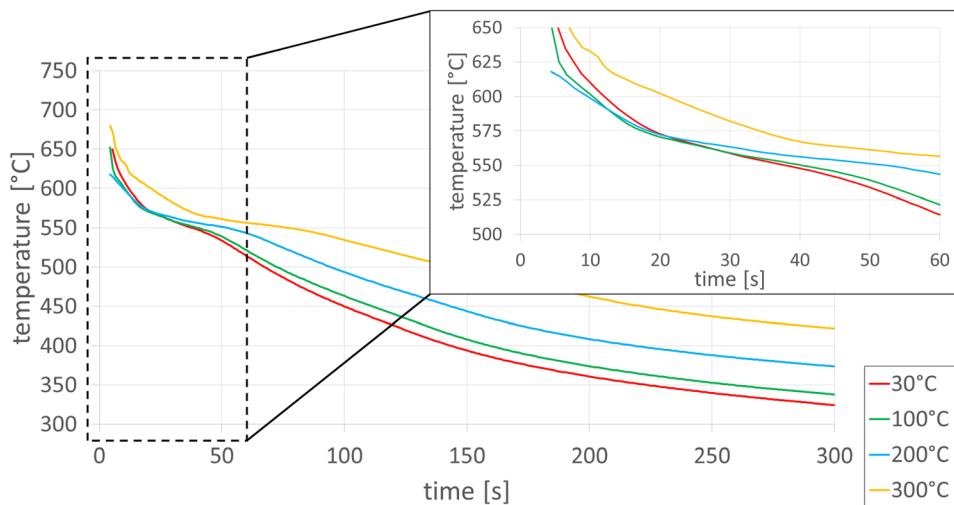
Figure 6. Cooling curves for upper, close to die (TC4) measuring position inside the melt.

dimensional radial heat flow from the melt either outwards to the die or inwards to the core. The lower measuring position is in a thinner-walled area where heat is dissipated on both sides via the outer copper insert and the inner steel core. This leads to comparatively high cooling rates in this region. The upper measuring position is also characterized by a direct heat dissipation via the outer copper insert, but is located next to a mass accumulation of the casting, due to which this region has a larger melt volume and does not dissipate heat to an inner core. As a result, this region has comparatively lower cooling rates.

The difference in the cooling rates is clearly visible when comparing the graphs of Figures 5 and 6, since low temperatures are reached much faster at the lower measuring

position. The same applies to the solidification times, which at the lower position are between approx. 15 and 35 s, depending on the die tempering, while the range for the upper position increases to approx. 40–70 s. With regard to solidification, it is also evident that the characteristics of eutectic solidification, consisting of primary and eutectic solidification, are generally recognizable. Especially at the lower measuring position with its higher cooling rates present there, the exact evaluation of the primary solidification is often difficult, since the temperature data recorded by the measuring instrumentation correspond only to the average of the values measured in a 1.1 s time interval, in order to counteract the existing measuring noise. Thus, the rather subtle changes in the cooling behavior during primary solidification cannot be

resolved with high accuracy and as a consequence temperature data of the following evaluation of the thermal analysis with regard to the liquidus temperature are only given as an integer. The eutectic solidification, on the other hand, is clearly recognizable for all measurements, even if only in a few cases a stable plateau is reached, or clearly recognizable minima/maxima are present in the temperature course. At a tempering level of 300 °C at the lower measuring position, all characteristic points of eutectic solidification can be identified. In all other cases, the characteristic areas of eutectic solidification can be identified, but without significant extreme values. The cooling is only slowed down by the solidification effects, with usually no discernible recalescences. Nevertheless, the key data defining solidification can be determined by performing a thermal analysis.

Thermal Analysis of Solidification

First, the characteristic temperatures of the liquidus temperature T_{liq}, the eutectic temperature T_{eut} and the temperature of the solidification end T_{end} are determined and discussed. As a comparison, a Calphad calculation for an AlSi7Mg0.3 alloy via ThermoCalc (using the TTAL8 database) is used to determine the equilibrium temperatures resulting in $T_{liq} = 615.38\,°C$ and $T_{eut} = 574.75\,°C$. The liquidus temperatures for the respective measuring position and die tempering are shown in Figure 7. The line shown there for the liquidus temperature according to thermodynamic equilibrium can also be used to estimate the respective undercooling. First, the data of the liquidus temperature for the upper measuring position are discussed. Here, a nearly uniform result for all temperatures and thermocouple positions is present. The determined liquidus temperatures almost correspond to the equilibrium temperature. A change in die tempering has nearly no measurable influence. The general effect of cooling via the outer insert can only be described as a reduction in the liquidus temperature by approx. 1 °C when comparing the middle and close to die thermocouple to the far from die

thermocouple position. In order to describe this influence more precisely, however, the measurement instrumentation lacks sufficient accuracy. Generally, it can be stated that the effect of a one-sided cooling in an area with a high melt volume has hardly any effect even on close to die regions in respect of the liquidus temperature and that even a variation of the temperature control has no significant influence here.

For the lower measuring position, the result is different. This can be attributed to both the fact that there is a smaller melt volume in the lower area, which is directly affected by heat removal, and to the fact that there is heat dissipation on both sides via the outer die and the inner core. The higher cooling rates resulting from this, as expected, are reflected in the resulting liquidus temperatures, which are lower and exhibit correspondingly higher undercooling in comparison with the upper position. A difference in tempering influence between the measuring position on the die/core side and the middle thermocouple in between exists. For the middle measurement, liquidus temperatures which are a few °C below the equilibrium temperature can be found. There is also a slight dependence on the die tempering, since for the 200 and 300 °C level a T_{liq} higher by 1 °C compared to the 30 and 100 °C tempering levels can be determined. A similar behavior can be derived from the die and core side measurements, which each have a distance of approx. 3 mm from the respective interface. Here, an undercooling of up to approx. 15 °C is present. The position of the thermocouple on the die side shows a higher undercooling than for the core side. This effect can be explained by the proximity to the respective interfaces as well as by the lower melt volume compared to the upper measuring position. The respective areas are directly affected by the heat extraction, and the effect of dissipated heat is more pronounced because of the smaller melt volume than for an area where an identical heat extraction on a larger melt volume results in smaller differences. The fact that the die side shows the stronger undercooling can be explained via the active cooling of the outer inserts, while the inner core does not have any active cooling and
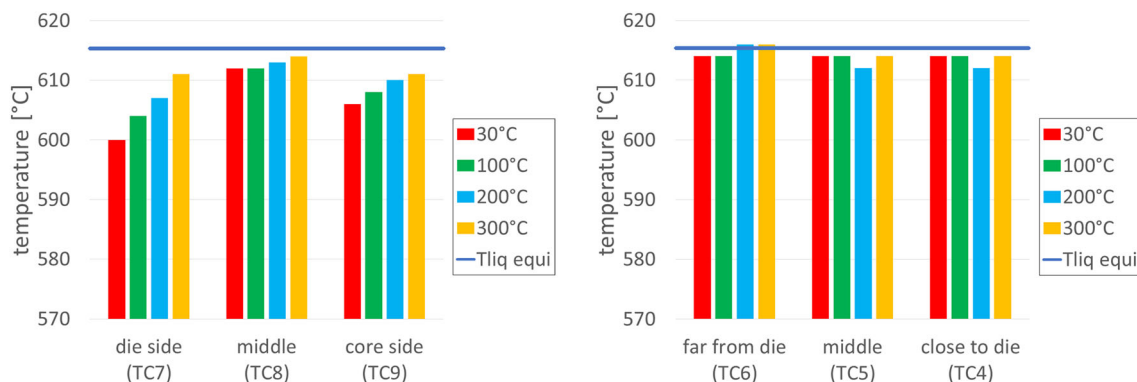
Figure 7. Start of primary solidification (liquidus temperature) at lower (left) and upper (right) measuring position.

therefore heats-up faster and heat dissipation in succession is lower in comparison with the outer die. The influence of the tempering levels also shows a clear difference in the liquidus temperatures, and changes of up to approx. 5 °C can occur between the individual settings. The level of the liquidus temperature can therefore be influenced in thinner-walled areas (in the given case a wall thickness of approx. 16 mm is present).

In general, however, the problem of the primary solidification evaluation lies within the high cooling rates, which in the lower area of the bowl can reach values of 10 °C/s. The thermal inertia of the thermocouples together with the evaluation methodology of a thermal analysis, which tries to find—for the given case—a relatively small change in the temperature curve, a distinct inaccuracy in the determination of the liquidus temperature exists. Defining the extent of this inaccuracy can hardly be done though. Hence, the declaration of liquidus temperatures only as integers instead of real numbers is chosen. Since the cooling rates decrease in the further course of the casting process, the evaluation of the other characteristic temperatures is not affected by this problem. The results discussed for primary solidification should therefore be understood more as a trend than as reliable numerical values.

For the evaluation of the eutectic temperature, the upper measuring position will be discussed first (cf. Figure 8). An influence of the copper insert on the close to die area can again be seen, but this time to a much greater extent with a lower eutectic temperature than at the other two thermocouples due to higher near die cooling rates. The middle and far from die measurements show basically similar eutectic temperatures for a 30 °C tempering. Regarding the far from die position, it is not influenced at all by different tempering levels. A dependence for middle and close to die positions, however, is present leading to decreasing T_{eut} for increasing tempering levels. This contradicts the expectations, since a higher temperature should result in lower cooling rates and thus less undercooling would have been expected instead of rising ones. Considering a successful Sr

refinement with accompanying depression compared to the eutectic equilibrium temperature in gravity die casting, an undercooling of approx. 11 °C is reasonable. However, finding the distinctive points for a thermal analysis in a cooling curve proves to be difficult in eutectic solidification at very slow cooling rates. As a result, the eutectic temperatures for 200 and 300 °C can be evaluated as too error-prone in the context of the present evaluation to still have sufficient precision. As a result, the analysis clearly can show the possibility of a noticeable undercooling by one-sided cooling of a larger melt reservoir up to approx. 6 mm distance from the mold. For positions more than 10 mm away from the interface, no fundamentally increased undercooling can be expected. Up to distances in these dimensions, a change in the tempering can still have an influence. At a distance of 18 mm from the interface at the latest, the influence of the tempering can be regarded as negligible.

The evaluation of the lower measuring position shows that this finding cannot be transferred to a thinner-walled area with two-sided cooling. Compared to the upper measuring position, a higher undercooling can be determined due to the higher cooling rates. Within the lower measuring position, the thermocouples on the die and core side again show an analogous behavior that deviates from that of the middle. In the middle, there is basically less undercooling, since the position of the thermocouple is not in immediate vicinity of a mold interface. Furthermore, the influence of tempering is again small, leading to minimally increased eutectic temperatures with increasing insert tempering. Both the die and core sides show higher undercooling, i.e., a lower eutectic temperature due to the higher cooling rates. A change in tempering at these two positions shows a clear effect on the eutectic temperature as an increased tempering level would cause an increase in T_{eut} which is in line with the associated change in the cooling rate and matches the respective expectations. While for primary solidification, the die side measurement showed noticeably higher undercooling than for the core side measurement, this difference no longer occurs for eutectic solidification.
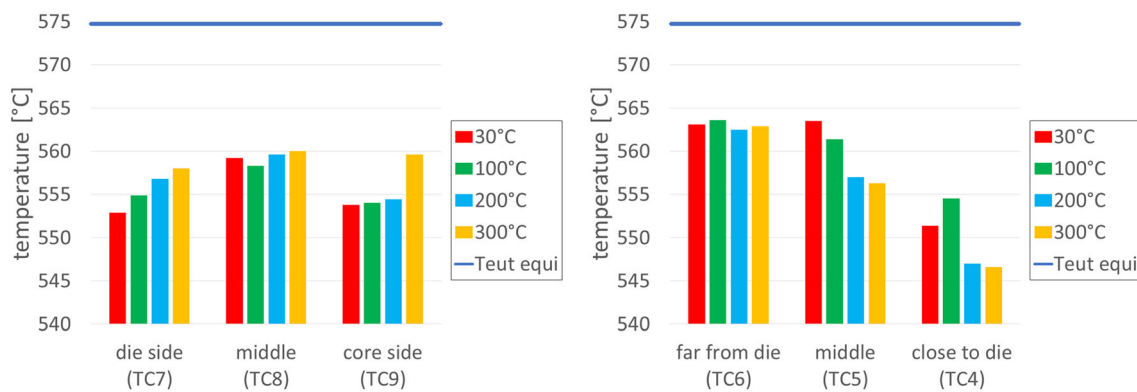
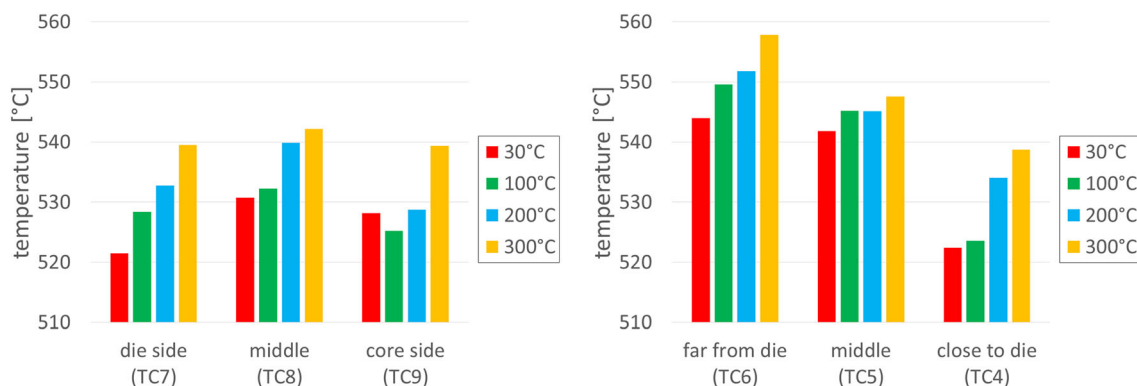**Figure 8. Eutectic temperature for lower (left) and upper (right) measurement position.**

In general, the undercoolings are at a similar level, whereby the increase in the eutectic temperature for the 100 and 200 °C tempering on the core side is only slight, but for 300 °C it ends at a level that would correspond to a trend similar to the increase on the die side. However, there is also the possibility that the 300 °C evaluation on the core side represents an outlier and that the influence of tempering the core side is only minimal. Since only the die side is actively cooled, there is the possibility that there is only a minimal influence on the core side by tempering, similar to the influence in the middle, which would correspond to the results of the upper measurement. The generally similar undercooling levels on the die and core side, which in comparison with those of primary solidification has approached each other, could be explained by the fact that as solidification progresses, the influences of the geometric conditions begin to gain importance. The volume shrinkage during the liquid–solid phase change causes the formation of an air gap on the die side, since the casting shrinks with respect to the outer geometry. On the side of the inner core, the casting shrinks onto the core and, due to the increasing contact pressure, leads to increasing casting-core contact and thus improved heat transfer. The conforming of the undercooling levels during eutectic solidification compared to primary solidification could be due to this phenomenon, in which although active cooling is present on the outer die side, the air gap formed reduces the heat transfer, while on the inner core side the heat transfer is improved as a result of the increasing contact pressure, but the heat conduction is slowed down due to lower temperature gradients as result of a heating of the inner core over time.

Finally, the temperature at the end of solidification is evaluated as the last significant temperature of the thermal analysis (cf. Figure 9). At the upper measuring position, there is a clear influence of the proximity to the die. The lowest temperatures for the end of solidification can be found at the close to die position, the highest (approx. 20 °C higher) at the far from die position. At the middle thermocouple in between, an intermediate value

approaching the value farther away from the die is present. This indicates that the end of solidification, i.e., the phase change of the last areas with residual melt, which in most cases is present in the interdendritic spaces, appears to be strongly kinetically inhibited. This way with faster removal of heat, complete solidification occurs at lower absolute temperatures than in regions with lower cooling rates. The evaluation of the influence of die tempering on the solidification temperature shows that a change in this case affects the solidification temperature at all three thermocouple positions. A higher tempering temperature corresponds to an increased T_{end}. The fact that in this case the tempering has an effect that reaches deep into the component also indicates a kinetic inhibition of the final solidification, while the relatively large jumps in the temperature between the respective tempering settings of often approx. 5 °C can be attributed to the fact that the release of latent heat no longer plays an important role thus pronouncing the immediate effects of tempering. During eutectic solidification in particular, a temperature plateau often forms due to the released latent heat, which counteracts cooling. This effect is no longer of major importance toward the end of solidification, so that greater differences between the individual tempering settings would generally have to be expected.

An evaluation of the conditions at the lower measuring position shows a behavior which is analogous to the explanations at the upper position. The thermocouples positioned near the die and core side show lower temperatures for the solidification end, since this is where the highest cooling rates are present. The middle measuring position without immediately adjacent die shows slightly higher temperatures in comparison. Analogous to the upper measuring position, there is also an influence of the tempering settings at all three thermocouples, whereby a higher temperature also leads to an increased T_{end}.

In addition, the total time of solidification Δt can be reviewed, which elapses between the beginning of

Figure 9. End of solidification (solidus temperature) for lower (left) and upper (right) measuring position.
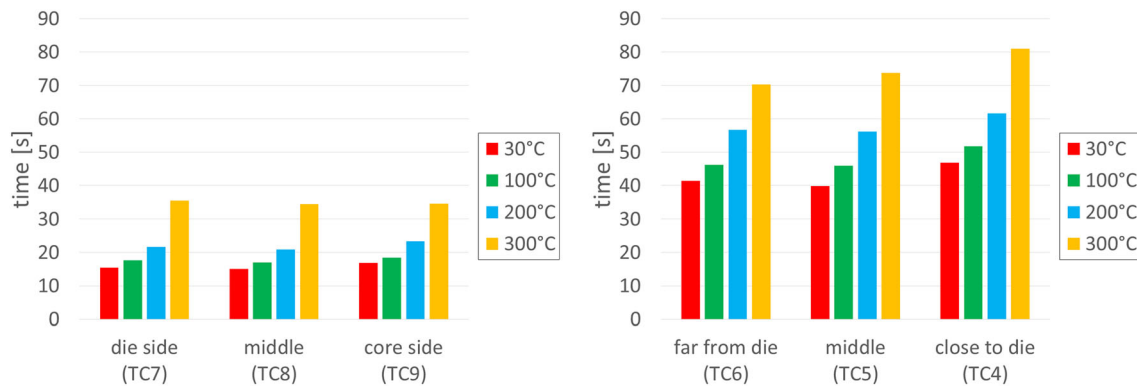
Figure 10. Length of solidification interval (solidification time) for lower (left) and upper (right) measuring position.

solidification at T_{liq} and the end of solidification at T_{end}. This is shown in Figure 10. For the upper measuring position, it can be seen that, contrary to expectations, the higher cooling rate in the close to die area is connected to a longer solidification time than in the middle and far from die position, which have almost identical values. However, the difference is only a few seconds and can therefore be neglected in the context of the inaccuracy of the thermal analysis method. The much more significant influence on the solidification time lies in the die tempering. Here, the solidification time can be almost doubled by increasing the oil temperature from 30 to 300 °C with approx. 40 s compared to 70 s solidification time, respectively. At the lower measuring position, the solidification time Δt, which results for the evaluation at the three thermocouple positions, can be described as uniform, since quasi-identical values are always present. The striking influence of the die temperature also is evident analogously to the discussion for the upper measuring position.

Thus, the length of the solidification interval is strongly dependent on the die tempering, which ensures different cooling rates. This is examined in more detail by comparison with Table 2. The table shows the percentage

increase in the solidification interval per increased °C between the four tempering variants of the die. For the upper measuring position, for all three positions of the thermocouples examined, it is shown that each increase in tempering has a greater influence on the solidification time the higher the temperature already is. The change from 200 to 201 °C can have an effect more than twice as high as the change from 30 to 31 °C.

As a final consideration for the melt's cooling rate and how it is influenced by the die tempering, the total cooling rate, which on average must be available in order to cool the melt down by the temperature difference of the solidification interval within the solidification time, is evaluated. Figure 11 shows the total cooling rates for the respective positions. For both measuring positions, a uniform behavior can be seen—the cooling rates are nearly the same for identical tempering temperatures. The variation of tempering itself causes significant changes in the cooling rates with the trend of lower cooling rates for increased die temperatures. The absolute values at the upper measuring position are less than half as high compared to those at the lower measuring position. On the one hand, this can be attributed to the lower melt volume in the lower area of the

Table 2. Increase in Solidification Time Δt in % Per Increased °C of Tempering Temperature

| Change in tempering	Die side			Middle			Core side		
	30 °C → 100 °C	100 °C → 200 °C	200 °C → 300 °C	30 °C → 100 °C	100 °C → 200 °C	200 °C → 300 °C	30 °C → 100 °C	100 °C → 200 °C	200 °C → 300 °C
Δt increase per °C bottom (%)	0.2	0.23	0.64	0.2	0.23	0.65	0.13	0.27	0.48
	Far from die			Middle			Close to die		
Δt increase per °C top (%)	0.17	0.23	0.24	0.17	0.22	0.31	0.15	0.19	0.31
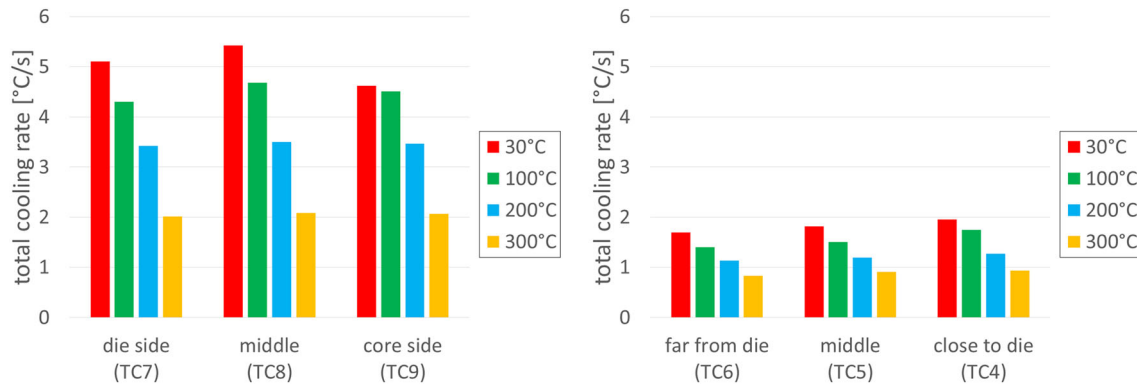
Figure 11. Total cooling rate determined over the entire solidification interval for lower (left) and upper (right) measuring position.

casting, whereby the same energy output leads to a higher temperature change compared to the upper area with higher volume. On the other hand, the two-sided cooling via the outer insert and inner core in the lower position contributes to this. As a rule of thumb, it can be stated that the cooling rate in the lower range decreases by an average of approx. 1 °C/s with an increase of 100 °C in tempering, while for the range of the upper measuring position it is only approx. 0.4 °C/s. Set in relation, this corresponds to a relative change in the rates of 20–33% for both measuring positions. Tempering in thinner-walled areas therefore makes a much greater difference, which could be even greater if both sides would be actively cooled. In the given case, only the outer copper inlet is tempered, while the inner steel core has no direct cooling. Tempering of the core thus should lead to a further increase in cooling rates. In a casting process, it is therefore possible to significantly change the cooldown of thinner-walled areas via tempering

with comparatively minor absolute changes in thick-walled areas.

In addition to the consideration of the thermal conditions just at the given thermocouples, the spatial influence of tempering in the entire casting also is considered. The results of the thermomechanical simulation are used in order to describe the temperature distribution within the melt starting from the interface between the casting and the outer die (or air gap) up to a depth of 50 mm into the casting. The moment at which the melt inside this 50-mm-thick volume has completely solidified is selected as the process time to eliminate the influence of latent heat that has not yet been completely released and the upper measuring position will be further evaluated with its direct influence of the cooled outer cooper insert. Figure 12 shows the temperature curves within the casting as well as the associated solidification times. The positions and
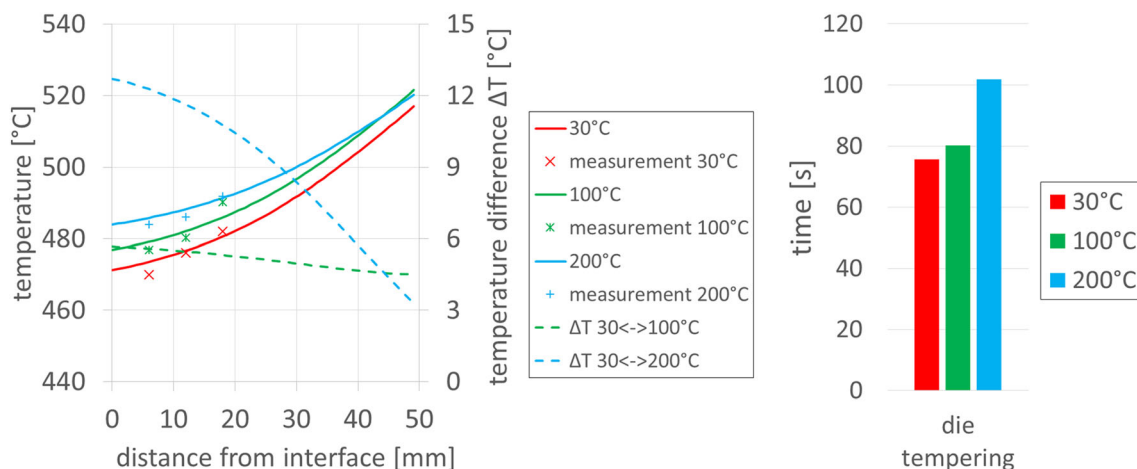
Figure 12. Melt temperature as a function of distance from the interface at the time of total solidification of the outer 50 mm (left) and time of total solidification at 50 mm distance from the interface (right).

measured values of the thermocouples from the experiment are also indicated. Usage of the simulated results allows the consideration of a much larger range than possible by the experimental measurement and reaches up to the interface. In general, the investigated range solidifies at the earliest for a die tempered at 30 °C and thus leaves most of the time for a further cooling below the solidus temperature. For the 200 °C tempering, the largest solidification time of the investigated temperatures applies, leaving less time for further cooling below the solidus temperature and therefore the highest absolute temperature values can be found here. The comparison of the temperature curves shows that a lower tempering directly at the casting surface (i.e., at a depth of 0 mm) ensures lower temperatures, whereby in the given case an increase of 7 °C per 100 °C increases in tempering level can be expected. If we look at areas further away from the interface, the temperatures increasingly converge and at a depth of 50 mm, the difference between the highest and lowest temperature is more than halved at approx. 4.5 °C. Temperature differences ΔT in relation to the 30 °C curve are also shown in Figure 12. A difference in the behavior of the temperature curves can be seen here. When comparing the 30 °C and 100 °C curves, an almost parallel course in which the temperature difference continuously decreases from 5.7 to 4.5 °C can be determined. For a tempering of 200 °C, a similar behavior can be seen near the interface, but the temperature difference decreases at an ascending rate for further distances from the interface. So, the temperature levels at a material depth of 50 mm are almost equal to those of 100 °C tempering.

Dissipated and Latent Heat

In order to further describe the influence of tempering on the spatial cooling within the melt, the data shown in Figure 12 are used to make a statement about the absolute heat energy dissipated. On the basis of the known size of the heat capacity, density and latent heat of the aluminum alloy, the dissipated heat energies per mm³ melt volume can be described via multiplying heat capacity by density and subsequent integration via the predominant

temperatures (starting from a maximum melt temperature of 700 °C). This is shown in Figure 13. The graph on the left shows the resulting energies for the three tempering levels. As was to be expected, most of the energy is dissipated for the lowest level of 30 °C. The resulting curves are very similar, but the graph on the right in Figure 12 shows them in a different relation. In addition to the total heat energies dissipated, the ratio of latent heat is also shown here. It can be seen that in the given case the latent heat represents about half of the dissipated energy. Since a complete solidification is present at all positions, it is equally large for all considered cases. This underlines the importance of the energies released during the phase change. However, the given illustration also makes it clear that although tempering has an influence on heat extraction which can lead to noticeable differences in some characteristic values (cf. the discussion of the thermal analysis), the absolute amount of heat that the system can dissipate is rather slightly influenced by tempering—at least in areas such as the one investigated here with gap formation between the casting and the die.

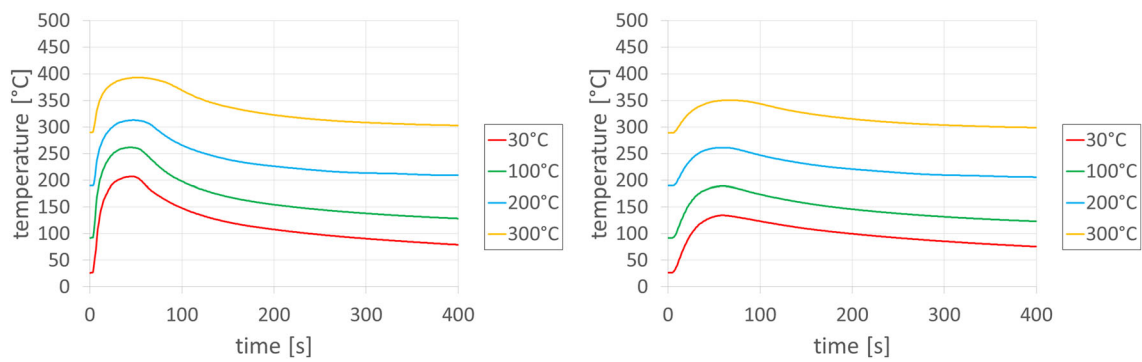### Temperature Development in Outer Die and Inner Core

In addition to the temperatures in the melt, the thermal effects in the copper inserts and the steel core will also be discussed. Figures 14 and 15 show the temperature curves in die and core for the close to melt and far from melt measurements of the thermocouples (cf. Figure 2). Evaluating the results for the core shows a pronounced maximum in the near-melt measurement temperature curves. This extremum no longer occurs for a far from melt position. A maximum can also be found for the insert evaluation at a close to melt measuring position. In contrast to the core, this also remains the case with a far from melt measurement—albeit to a lesser extent. Figure 16 shows the maximum temperatures present in each case. The expected trend of a higher tempering leading to a higher temperature maximum is present here. The differences between the individual tempering levels are greater for the die than for
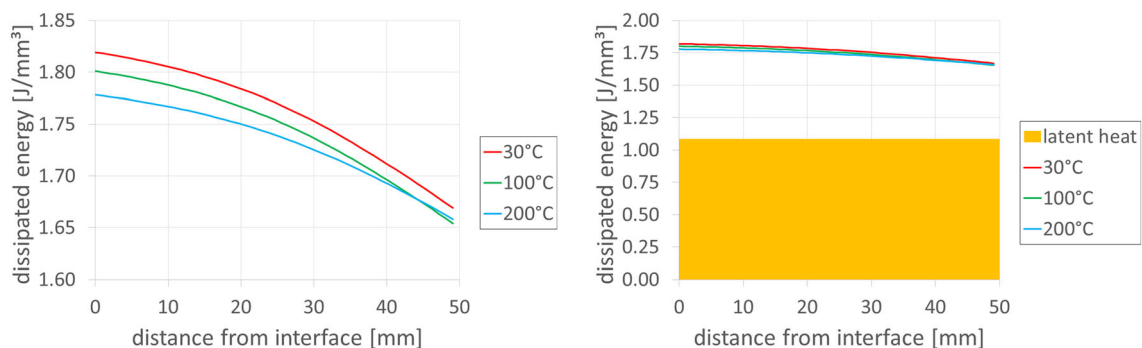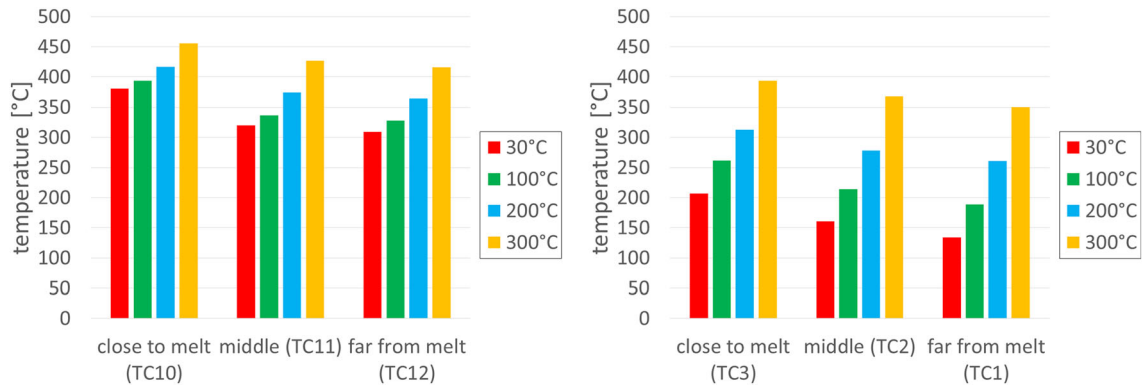

Figure 13. Dependence of dissipated heat energy from the applied tempering.
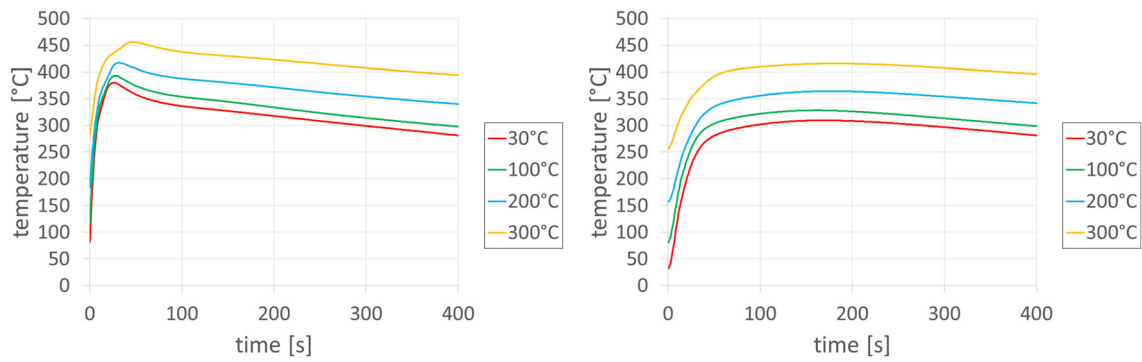
Figure 14. Temperature development inside the non-cooled inner core at close to melt (left) and far from melt (right) measuring position.


Figure 15. Temperature development inside the actively cooled outer die at close to melt (left) and far from melt (right) measuring position.
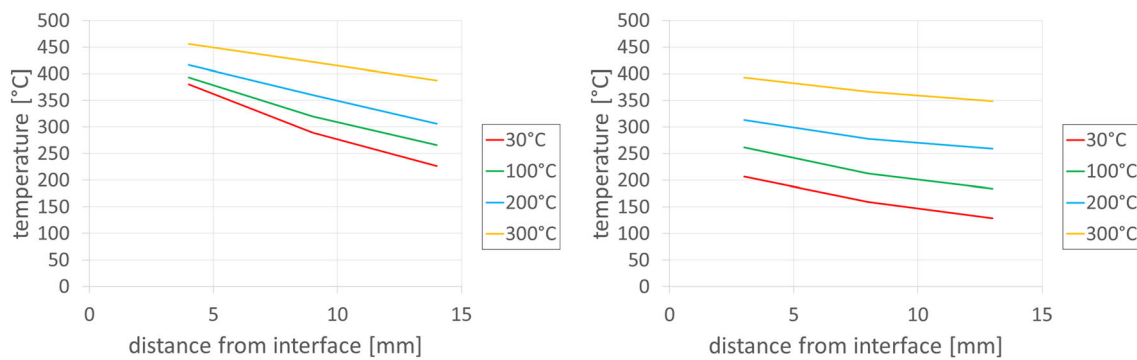

Figure 16. Maximum temperature inside core (left) and die (right).

the core with a temperature increase of 100 °C leading to an increase in maximum temperature of approx. 60 °C. At the core, the respective increases are only about half as large. Here, however, the absolutely higher maximum temperatures can be seen, which is due to the lack of active cooling which would keep the core temperatures at a lower level. Therefore, the once reached maximum temperature remains almost the same or cools down only very slowly in the case of the near-melt region. For the actively cooled

die, a cooling down to the original temperature values occurs after reaching the maximum. The higher the tempering level, the faster the die temperature approaches the original value. This is illustrated in Figure 17. Here, the temperature difference between the measured maximum and the set tempering level is plotted. For the actively cooled outer die, it is shown that the absolute temperature difference is smaller for higher tempering levels. The return to the initial temperature level can therefore take
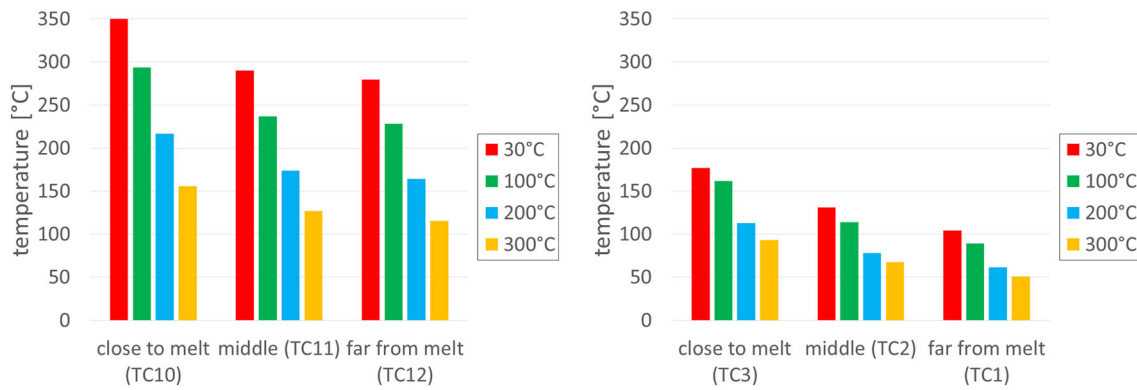
Figure 17. Temperature difference between chosen tempering level and maximum temperature for core (left) and die (right).

Figure 18. Spatial temperature distribution at time of maximum temperature inside the core (left) and the die (right).
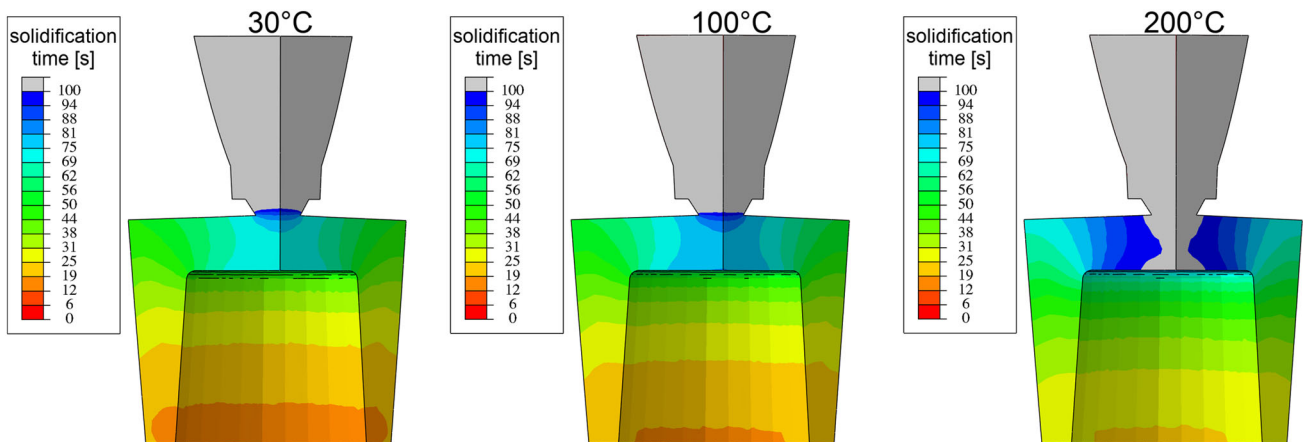
Figure 19. Absolute solidification time for a 30 °C (left), 100 °C (middle) and 200 °C (right) tempering level.

place faster than at lower temperatures, since a lower absolute temperature difference must be cooled down. Identical tendencies can be seen on the inner core, but in the absence of active cooling, these are more pronounced, resulting in higher absolute temperature differences for the core.

Figure 18 shows the spatial temperature distribution in the outer die and inner core at the time of the maximum close to melt temperatures. In comparison with the similar consideration for the melt (cf. Figure 12), there no longer is a curve, but a quasi-linear relationship. The rate of temperature change is almost identical for both die and core, and a

temperature decrease of approx. 50 °C per 10 mm material can be observed.

Influences of the cooling medium, which increasingly heats-up as it passes through the channels, can be neglected. The oil temperature, measured inside the heating/cooling unit when returning from the copper inserts, showed a quasi-identical heating independent of the chosen tempering level of approx. + 5 °C during the solidification representing the period with the highest heat fluxes.

Progress of Solidification

Although many characteristic data for the solidification can be determined from the experimentally obtained cooling curves and their analysis, information about the solidification process can only be obtained punctually this way due to the limited locality of the measurements. In this respect, the results of the numerical solidification simulation can be used to extend the available information. Figure 19 shows the local solidification time on the entire casting. As can be seen in particular from the representation of the solidification time at 30 °C tempering, the solidification in the cup does not only begin from bottom to top, but the areas in contact with the inner core solidify prior to regions in the immediate vicinity of the outer die. This can be explained by the lower heat dissipation on the insert side due to the air gap occurring there. With regard to the influence of die tempering on solidification times, it can be noted that the difference between the 30 and 100 °C level does lead to a slower solidification for the 100 °C case which is reflected by a difference of about one color gradation in the figure, which corresponds to an extension of the solidification time of approx. 6 s. A comparison between 100 and 200 °C tempering level, on the other hand, shows a greater influence on the solidification time, since the color gradations differ by several levels on the scale, especially in the upper range with the final solidification of the residual melt. The indicated time period of
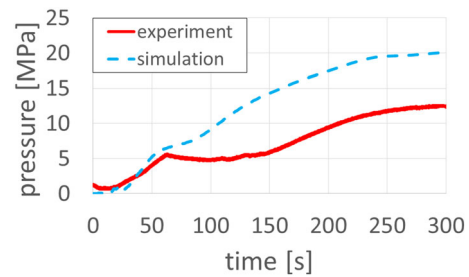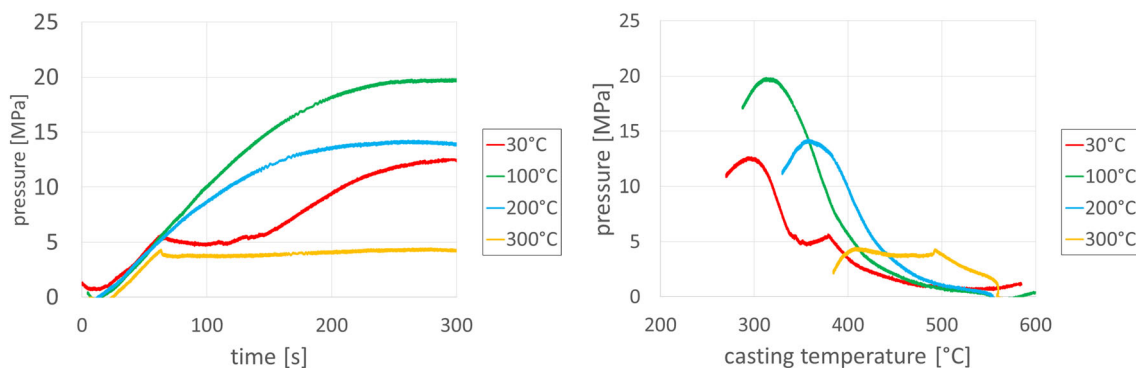

Figure 21. Contact pressure development at the inner core for 30 °C tempering taken from experimental measurement and simulation.

100 s also is insufficient to enable a complete solidification for the case of 200 °C tempering as the region below the sprue feeder has not yet solidified completely. This can be attributed to the fact that heat conduction is increasingly slower with a lower temperature gradient. Thus, at 70 or 100 °C change in tempering temperature, there is a rather similar absolute change in temperature compared here while the relative change in the temperature gradient is higher when the tempering level is increased from 100 to 200 °C, which is why the effects on the solidification time are higher than when the temperature control is increased from 30 to 100 °C.

Contact Pressure Development

With the cooling behavior having been discussed, the contacts of the casting to the outer die and to the inner core are now examined.

Figure 20 shows the development of the contact pressure at the inner core as a function of time and cast metal temperature, respectively. As the casting shrinks onto the inner core, increasing pressures occur during solidification or further cooling. The measurement results show a distinctive break in their trend for the 30 °C and 300 °C curves at a time of approx. 60 s. This is due to a movement of the

Figure 20. Development of contact pressure at the inner core on experimental measurement height level as function of time (left) and as function of casting metal temperature at the core contact interface (right).

measuring setup, which is prone to settling of the die parts as soon as stresses occur. A blockage of the quartz glass rod transmitting the forces of the pressure measurement (cf. Figure 1) can be the result. In case of the 300 °C measurement, the rod is completely blocked, which means that there is almost no recorded change in the pressure behavior during the test. In case of the 30 °C measurement, there is only a temporary disturbance until after a few seconds rising values for the pressure are recorded again. A comparison with the simulation as shown in Figure 21 shows that the course of the measured pressure, which increases again after stagnation, runs quasi-parallel to the simulated pressure development and thus that the additionally increasing pressures are measured correctly again. When comparing the pressure development for the different die tempering levels, a clear influence can be determined, even though the inner core itself is not tempered directly. During the first approx. 60 s process time, all curves show an almost identical course. However, this changes in the further course of the process. When using the simulated pressure curve at 30 °C and the measured curve at 100 °C tempering, it can be seen that the pressure development is very similar. Here, the highest determined pressure of approx. 20 MPa is reached. In comparison, the measured maximum pressure for the 200 °C level only reaches approx. 14 MPa with lower pressure rise rates compared to the processes with lower tempering levels and a shorter time span until the maximum pressure is reached. When comparing the contact pressure with the respective casting metal temperature at the interface, it can be seen that there is no uniform pressure increase in terms of a function of temperature (as the initial data for high casting metal temperatures all develops differently). Instead, a reduced tempering level ensures that the same pressure levels are shifted to lower cast metal temperatures until the pressure curves run almost parallel from a certain point. The shift in temperature between points of identical pressure for the different tempering levels is approx. 20 °C to the next higher/next lower variation. Tempering hence can influence the maximum applied pressure as well as the temperatures in the casting corresponding to a certain contact pressure. The reason for this can be traced back in
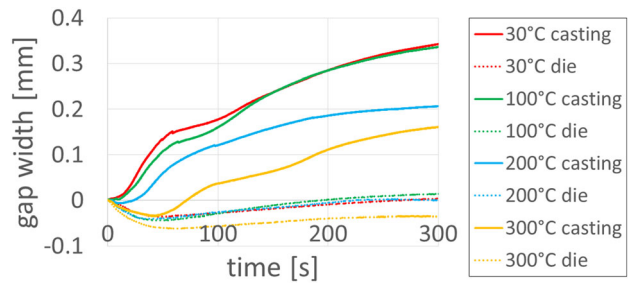

Figure 23. Share of die expansion and casting contraction on the total amount of displacement, i.e., gap width.

particular to the starting temperature of the inner core. Even if there is no direct initial heating, the inner core is indirectly heated during casting preparation by tempering of the outer die. Higher temperature levels result in a higher starting temperature of the inner core. When getting in contact with the melt, there is a correspondingly lower temperature difference, i.e., the core will experience less absolute heating and therefore expand to a lesser degree. Conversely, for the results of the 30 °C level taken from the simulation, this means that although it provides a good estimation of the pressure levels that occur, there is still room for improvement in the simulation model, since starting from the 100 °C measurement, slightly higher pressures for the 30 °C case would have to be expected with regard to the trend that can be expected from the experimental data.

Air Gap Development

Since the bowl is cylindrical in shape, its external dimensions shrink during solidification or further cooling. This creates an air gap along the casting surface toward the contact with the outer die. The development of the gap width as function of time and cast metal temperature is shown in Figure 22. A dependence of die tempering on the gap development can be seen. Lower tempering temperatures lead to increasing gap sizes which also form faster. However, as the casting metal temperature-dependent
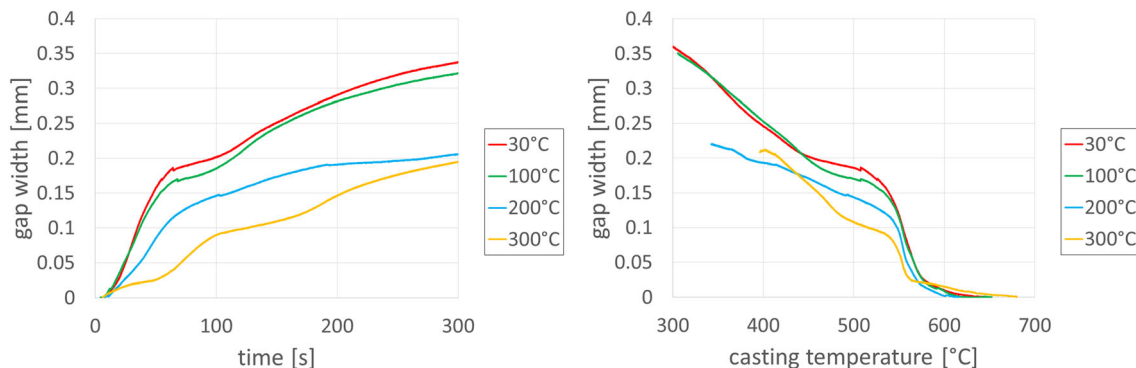
Figure 22. Development of gap width at the exterior face of the casting.

curves show, this is not a uniform process which gets slowed down in regard to time by the tempering. The comparison of the curves for the 30 °C and 100 °C levels shows a very similar course over time. If the associated gap width is compared with regard to the casting interface temperatures, the curves of these two tempering variants actually run almost congruently over wide ranges—only in the 450–550 °C range does the curve of the 30 °C tempering level have higher gap widths than for the 100 °C variant. The two other tempering variants investigated show no tendency to approach the graphs of 30 and 100 °C level at any position though. At the same temperature, they form smaller gap widths than a higher tempered variant with the exception of an intersection for the 200 and 300 °C level. One reason for higher gap widths with lower die temperatures could be the temperature difference between die and melt. A die that is colder at the start of the process will heat-up more strongly and expand accordingly. This would contribute to the comparatively high rate of change of the gap width at the beginning of the process. However, as Figure 23 shows, this assumption could not be confirmed. The splitting of the total gap into its share of die and casting movement shows that there is a trend toward high values for the expansion of the die at high tempering levels. In principle, the contribution of the die movement to the overall gap width is of high relevance only at the beginning of the gap development, since the absolute values achieved for its wall movements are clearly below those of the casting's walls movement. It can also be seen that after a maximum die movement has been reached, it begins to compensate itself again when the die starts to cool down again toward the initial temperature.

Furthermore, there would be the possibility that increased stresses could occur in the casting due to an increased cooling rate, which would contribute to increased deformation and result in higher gap formation. The idea of increased stresses also can be applied to the case of contact pressure on the inner core. Considering how close the curves for the gap width at 30 and 100 °C level are to each other transferring this behavior to the contact pressure

would explain the simulation results for contact pressure at the 30 °C level which came out to be at the same level as for the 100 °C measurement too.

Finally, it should be noted that the curve of the 30 °C tempering level shows a negligible jump at a time of approx. 60 s. This behavior of gap width development coincides with an identical behavior of the deviation in the pressure measurement at exactly the same time and thus supports a settling effect as reason for this while in contrast not having a significantly negative influence on the gap measurement.

Stress Evaluation

Since it is not possible to measure the stresses in the casting experimentally, the results from the thermomechanical simulation are used to evaluate the von Mises stresses in the casting. Figure 24 shows the stresses present at the position of the gap measurement as well as in the area of the pressure measurement. It can be seen that the von Mises stresses actually reach higher values faster with lower die tempering levels than for higher levels. This could therefore be a reason for the differences in interface temperature-dependent gap width and contact pressure behavior. However, Figure 25 shows a further evaluation of the von Mises stress to the respective casting metal interface temperatures. Here, no dependency of the die tempering can be derived, since all curves are nearly identical. However, for both contact pressure and gap width, a different behavior with regard to the cast metal interface temperature was found in connection with different die tempering levels. The effects of the stresses present in the casting cannot be the cause of these differences.

The same applies to the depiction of stress as function of contact pressure as shown in Figure 26. The resulting curves are virtually identical for the different tempering levels. Only the 200 °C curve shows a slight short-term
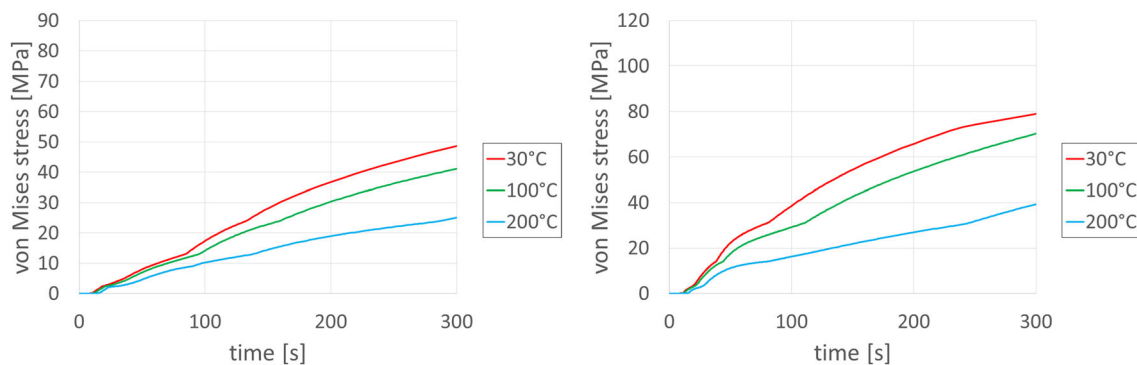
Figure 24. Simulated von Mises stresses at the point of gap width measurement (left) and contact pressure measurement (right) as function of time.
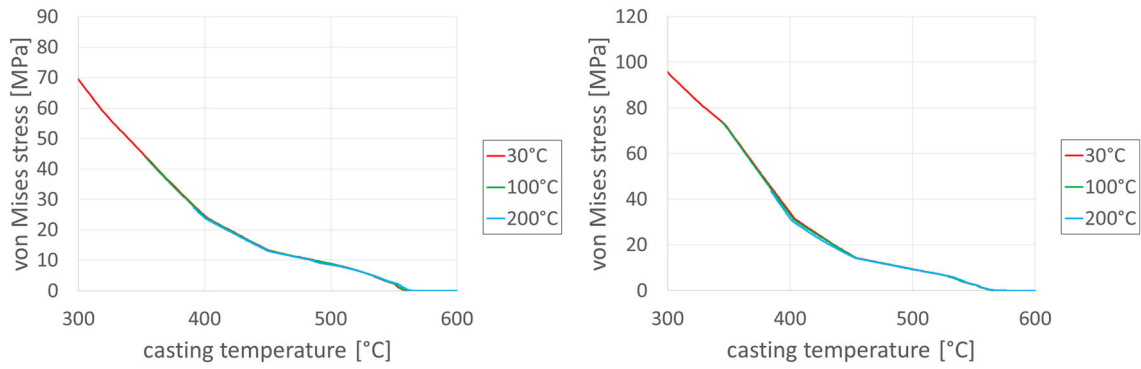
Figure 25. Simulated von Mises stresses at the point of gap width measurement (left) and contact pressure measurement (right) as function of casting metal interface temperature.
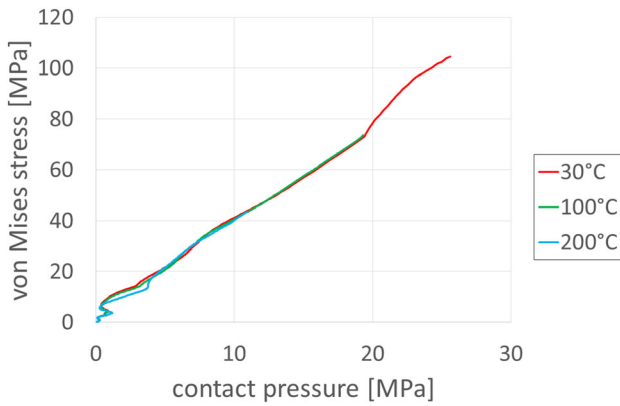

Figure 26. Dependence of von Mises stresses on contact pressure.

deviation at low pressures or stresses. However, since it is in the range of up to 4 MPa contact pressure, this represents a process stage where no large pressure differences have developed yet as was shown in Figure 20. For this reason, this deviation is of no further interest for the given discussion.

Shrinkage Behavior

Finally, the shrinkage behavior with regard to die tempering is to be discussed. The overall shrinkage behavior of the bowl geometry is shown in Figure 27 on the left. The shrinkage-induced gap formation toward the outer die as well as the constant contact with the inner core can be seen. It is shown that the upper part of the bowl geometry causes a locally larger gap in contrast to the lower parts of the component, where the inner core is present. This happens due to the different casting metal volumes whose shrinkage is responsible for the gap formation. Figure 27 on the right shows the gap widths along the entire outer wall according to the simulation after 300 s process time, starting at the bottom of the bowl as height zero. Up to a height of approx. 60 mm, where the inner core is present opposite to the outer die, a constant gap width can be determined even with increasing height along the outer wall. Subsequently, the influences of the massive casting area above the core (total core height = 85 mm) begin to affect the gap width. Increasing gap widths with higher positions on the outside of the casting can be determined.
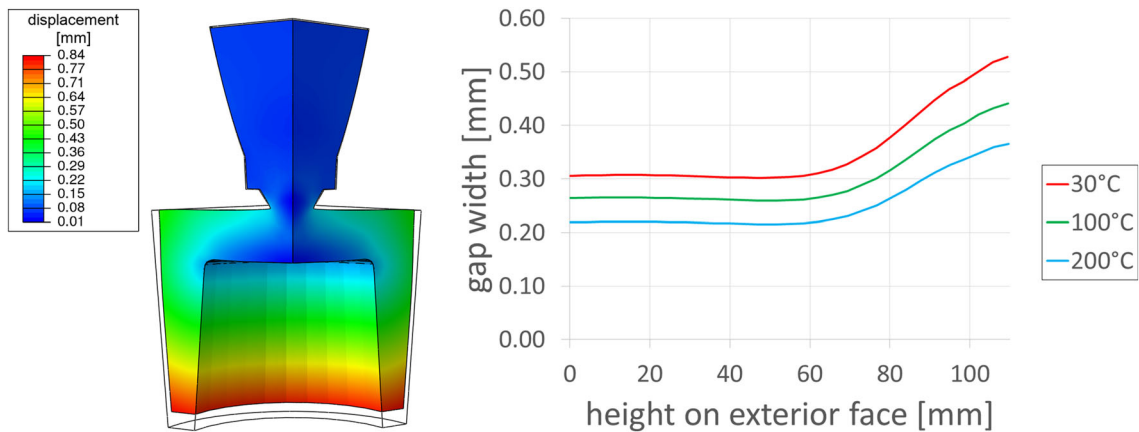
Figure 27. Displacement of the bowl geometry (left, visual amount of displacement on geometry increased by factor 10) and gap width along the exterior face of the bowl-shaped casting beginning from the bottom upwards after 300 s of process time.
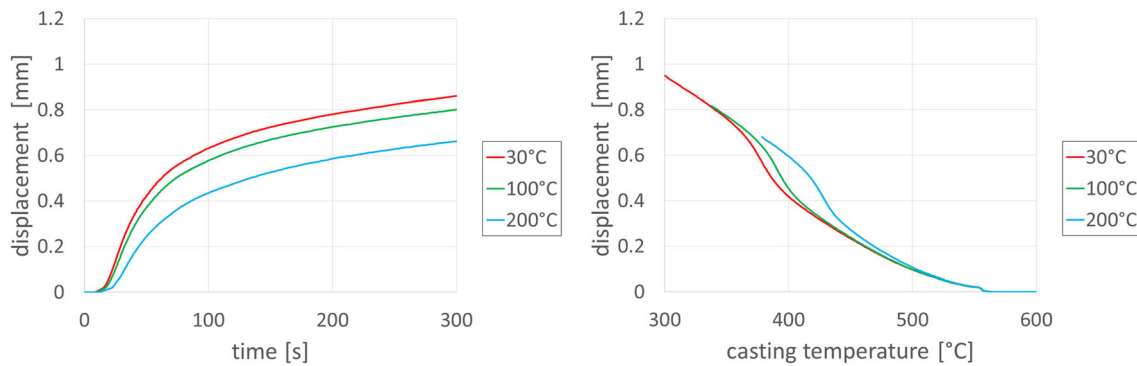
Figure 28. Displacement of bottom surface due to thermal contraction.

Furthermore, the movement of the lower bottom surface of the casting was investigated. The bottom surface will shift most significantly during the contraction of the component due to the high vertical dimension of the bowl. The bottom surface's shrinkage or upward displacement is shown in Figure 28. A temporal dependency of displacement on the different tempering levels can be seen. An increase in cooling rate due to lower die temperatures leads to a faster shrinkage that occurs thus matching the expectations toward this behavior. From the depiction of the displacement as function of the cast metal interface temperature, it can be derived that the start of the shrinkage and the low temperature behavior are basically identical for all tempering levels. The range immediately after complete solidification down to a cast metal temperature of around 350 °C, however, behaves differently. The result is an S-shaped curve whose slope is differently curved depending on the applied tempering. As already indicated in the examination of the von Mises stresses, there is no influence whatsoever on the final distortion of the component due to the die tempering, apart from the obvious connection that a higher contraction is achieved more quickly when achieving a faster cooling.

It may be necessary to extend the modeling in order to clarify the phenomena presented. For example, the cooling rate influences the course of the curve for the solid phase fraction development. In order to simulate these effects, the simulation model used would have to be extended by a cooling rate-dependent description of the development of the solid phase fraction. Another improvement in the modeling supposably would be the implementation of an extended density function. In the current implementation of the casting material density, a purely temperature-dependent description is used, but an approach of density as a result of the existing composition or phases could be developed for a more exact description of the local properties and the local course of the process. This may lead to influences in the thermomechanical simulation which currently are disregarded and might extend the delivered results.

Conclusion

Regarding the experimentally obtained results, the two regions examined represent the case of a one-sided cooling of a larger melt volume (upper measurement position) and the case of a two-sided cooling of a region with a smaller melt volume (lower measurement position). These different conditions lead to differences with respect to the performed thermal analysis and evaluation of gap width/contact pressure. The methodology of the thermal analysis leads to its intrinsic disadvantages as results evaluated this way are lacking in absolute precision, e.g., the search for points of inflection proves to be difficult to perform as processing data from an experimental measurement might lack in recording resolution or precision especially during process stages of high or very low change in temperature. Nevertheless, it still is a suitable method in the given case as it successfully can evaluate the influences of applying different settings for the oil tempering of the die. With the tempering levels ranging from 30 to 300 °C, the case of cooling at ambient temperature as well as a near maximum setting for an oil tempering (as oil evaporation occurring at around 370 °C has to be prevented) is covered representing the entire range possible for such a setup. While it is well known that a change in oil tempering temperature has a direct influence on the cooling rate, with a lower tempering level resulting in faster heat extraction, the actual influences on details of solidification or process parameters like gap width and contact pressure are not necessarily self-evident.

The following deductions could be drawn from thermal analysis:

Primary solidification:

- Solidification in regions with a large melt reservoir is nearly independent from different oil tempering settings due to aluminum's high thermal conductivity as even in close proximity to the die-melt interface the derived liquidus temperatures are close to equilibrium.

- Solidification in regions with a smaller melt reservoir can be influenced via changing oil tempering settings. At near interface positions (of up to approx. 10 mm), a distinct undercooling occurs which can be influenced by the applied tempering level.

Eutectic solidification:

- Influencing the solidification in regions with a large melt reservoir via oil tempering is possible resulting in a change of the local undercooling. The significant range for this effect amounts up to 6–10 mm distance from the die–melt interface.
- For regions with a smaller melt reservoir, the local undercooling can also be influenced via different oil tempering settings. The resulting difference in undercooling turns out to be smaller than for the primary solidification though.

End of solidification:

- The solidus temperature at the end of solidification can be strongly influenced in all regions via oil tempering of the die.
- This also applies to the temperature interval of the solidification, solidification time and total cooling rate.

This way it is possible to use certain tempering levels to affect only certain regions during solidification because as it was shown there exists the possibility to influence regions with different melt volumes. Planning for differences in heat balance primarily affecting regions close to the melt-die interface also can be done.

The evaluation of temperature development inside the die/core provides an estimation of the temperature increase inside either a die with or without active cooling via cooling channels. The given results for an aluminum casting process could be integrated during process planning and evaluating the amount of heat-up of the respective parts which could be limited by applying different tempering temperatures.

Finally, it is shown that the heat transfer-related parameters of gap width and contact pressures also can be controlled by applying different tempering variations. This thus indicates possibilities for a systematic approach for limiting (i.e., controlling) the amount of gap size or pressure formation on the respective parts.

Outlook

While this paper gives an idea of the general trends for certain influences and their potential, work needs to be done regarding the understanding of the mechanisms responsible for the actual changes in succession to a change in the thermal conditions. Using the results of the numeric simulation, certain factors possibly responsible were already investigated without being able to draw a final conclusion as to the main mechanisms responsible for the observed effects. Alternative phenomena might be considered in a future investigation as well as an extension to the present simulation model, which currently might disregard certain aspects important to stress and strain formation, as was proposed in the result's discussion.

REFERENCES

1. W. Schneider, D.H. StJohn, A.L. Greer, *Solidification Processing of Foundry Alloys: Mechanism of Grain Refinement of Aluminium—Almost All You Need to Know, Aluminium Alloys*, vol. 1 (Wiley-VCH, Weinheim, 2008)
2. J.E. Gruzleski, B.M. Closset, *The Treatment of Liquid Aluminum-Silicon Alloys* (American Foundrymen's Society, Schaumburg, 1990)
3. L. Wang, S. Shivkumar, Influence of Sr content on the modification of Si particles in Al–Si alloys. Metallkunde **86**, 441–445 (1995)
4. M. Di Sabatino, L. Arnberg, Effect of grain refinement and dissolved hydrogen on the fluidity of A356 alloy. Int. J. Cast Met. Res. **18**(3), 181–186 (2005)
5. D. Matisková, Š. Gašpar, L. Mura, Thermal factors of die casting and their impact on the service life of moulds and the quality of castings. Acta Polytech Hung **10**(3), 65–78 (2013)
6. L.Y. Zhang et al., Effect of cooling rate on solidified microstructure and mechanical properties of aluminium-A356 alloy. J. Mater. Process. Technol. **207**, 107–111 (2008)
7. L. Bäckerud, G. Chai, J. Tamminen, Solidification Characteristics of Aluminum Alloys—Volume 2: Foundry Alloys, AFS/Skanaluminium (1990)
8. D.M. Stefanescu, Thermal analysis—Theory and applications in metalcasting. Int. J. Metalcast. **9**(1), 7–22 (2015)
9. N. Wolff et al., Development of an A356 die casting setup for determining the heat transfer coefficient

depending on cooling conditions, gap size, and contact pressure. Materialwissenschaft und Werkstofftechnik **48**, Heft 12 (2017)

10. G. Laschet et al., Multiscale solidification simulation of an axisymmetric A356 component in die casting, in *Proceedings of the 6th Decennial International Conference on Solidification Processing (SP17)* (Old Windsor, UK, July 2017), pp. 576–580, SS Media, UK, ISBN 978-1-90854929-7

11. B. Pustal et al., Modellierung des Verzugs eines oberflächennah gekühlten A356 Gussteils mit unterschiedlichen Wärmeübergangs- und Erstarrungsansätzen. Gießerei Special **2**, 134–137 (2017)